Advances in Nano Research, *Vol. 19, No. 1 (2025) 29-39*
https://doi.org/10.12989/anr.2025.19.1.029

Effect of viscoelastic Foundation on the dynamic analysis of FG polymer nanoplates reinforced with graphene nanoplatelets

Abdelmadjid Lounis[1,2], Amina Attia[3], Abdelmoumen Anis Bousahla[2], Abdeldjebbar Tounsi[4,5], Abdelouahed Tounsi[*4,6], Houari Heireche[2] and S.R. Mahmoud[7]

[1]*Département D'Agronomie, Faculté des Sciences de la Nature et de la Vie et Sciences de la Terre, Université Djilali Bounaama de Khemis Miliana, Algeria*
[2]*Laboratoire de Modélisation et Simulation Multi-échelle, Université de Sidi Bel Abbés, Algeria*
[3]*Laboratoire d'Ingénierie et Développement Durable, University of Ain Témouchent, Faculté des Sciences et de la Technologie, Département de Génie Civil et Travaux Publics, Algeria*
[4]*Material and Hydrology Laboratory, University of Sidi Bel Abbes, Faculty of Technology, Civil Engineering Department, Algeria*
[5]*Mechanical Engineering Department, Faculty of Science & Technology, University of Relizane, Algeria*
[6]*Department of Civil and Environmental Engineering, King Fahd University of Petroleum & Minerals, 31261 Dhahran, Eastern Province, Saudi Arabia*
[7]*GRC Department, Applied College, King Abdulaziz University, Jeddah 21589, Saudi Arabia*

(*Received December 17, 2024, Revised February 17, 2025, Accepted June 30, 2025*)

Abstract. The aim of this study is to investigate the effect of viscoelastic support on the free vibration behavior of nanocomposite plates composed of functionally graded (FG) polymers and reinforced with graphene nanoplatelets (GNPs). A four-variable first shear deformation theory with nonlocal elasticity theory is used. By considering new shape functions, it is possible to explain why the transverse shear stresses and strains are parabolically distributed through the thickness of the plate and vanish at the top and bottom. Four alternative FG reinforcement patterns are used. The Halpin-Tsai model is used to calculate the effective material properties of the nanocomposite plates. Numerical results of nanoplate-FG polymer composite are compared with literature predictions to validate the results. A thorough parametric analysis revealed the influence of some important parameters on the dynamic behaviors of GNPs-reinforced FG polymer composite nanoplates, including nonlocal parameters, weight fraction, and parameters related to the viscoelastic basis.
Keywords: free vibration; graphene nanoplatelets; Halpin-Tsai model; shear deformation theory

1. Introduction

In recent years, two-dimensional materials such as graphene received considerable interest in engineering applications. Graphene nanoplatelets (GNPs) which are obtained by splitting and exfoliation of graphite have drawn the attention of many researchers to be used as reinforcement in polymer matrices (Dong *et al*. 2021). Generally, off-the-shelf GNPs are in micron-level sizes, but their size can be further altered according to the requirements of practical applications (Al Mahmud *et al*. 2021).

Today, the use of nano-scale reinforcing materials in base materials has simply evolved into an evolution in producing polymer composites with outstanding characteristics. Graphene nanoplates (GNPs) have shown extraordinary properties, and have been found to be an excellent filler material for increasing structural strength and other properties of composite materials (Liu *et al*. 2024). These characteristics come from actual atmospheric graphite sheets, alongside the exceptionally smaller size and large length-to-diameter ratio, making graphene a unique class of reinforcement for polymer matrix materials and also influencing the extraordinary compatibility and interaction between graphene nanosheets and polymer substrates (Liu 2020). Even though, advanced polymer nanocomposite has excellent mechanical, thermal, natural and innovative qualities due to the range and dispersion of low loadings of GNPs. Furthermore, GNP-reinforced "advanced" polymer nanocomposites have exhibited improved mechanical properties, thermal properties and other heritage characteristics due to the large aspect ratio and potent interfacial adhesion with polymer matrices (Liu *et al*. 2021). Polymer nanocomposites containing multi-functional GNPs are being developed to the better of simple homophony at present and making polymer science more crispy, conservational, and applicable, and also advance specializing and innovation throughout economic importance and market profitability for the various industries related to structural composites. The production and characterization of nano-composite materials involve a variety of synthesis techniques and analytical methods that enhance their unique properties for diverse applications. Understanding these methods is crucial for optimizing the performance of nanocomposites in various fields (Su *et al*. 2023, Xia *et al*. 2024, Jayakumari *et al*.2024)

An accurate model of structures and their vibration analysis are of utmost importance in various engineering fields, including civil, mechanical, aeronautical, marine,

*Corresponding author, Ph.D., Professor,
E-mail: tou_abdel@yahoo.com

ISSN: 2287-237X (Print), 2287-2388 (Online)

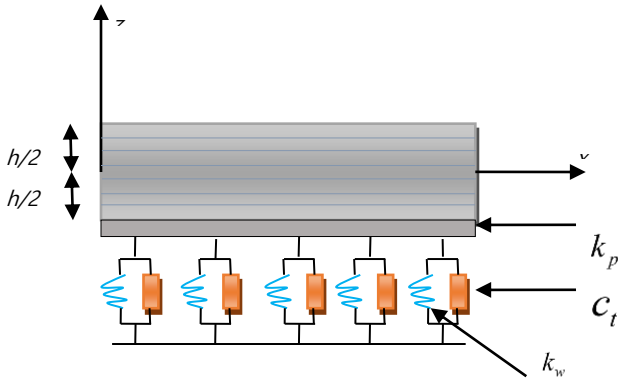

Fig. 1 GNP-reinforced FG nanoplate

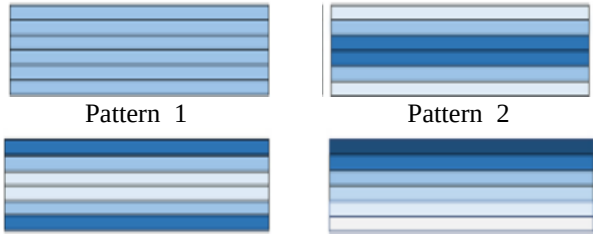

Fig. 2 Patterns of FG materials

and chemical engineering (Zhang *et al*. 2022). The theoretical, analytical, numerical, and experimental investigations about GNP-reinforced polymer nanocomposites have been investigated extensively in the works (Yang *et al*. 2017, Arefi *et al*. 2020, Ebrahimi *et al*. 2020, Mohammad-Rezaei Bidgoli and Arefi 2021, She *et al*. 2021, Afshari and Adab 2022, Ghasemi *et al*. 2023).

Like other nano-scaled materials, GNP-based polymer composites have a potential difference, and the mechanical properties like Young's modulus, yield strength of GNP-reinforced polymer materials vary, depending on the preparation process of the nanocomposites and local characterized parameters of GNPs in polymer nano-composites. Nanocomposites with exquisite mechanical, thermal and electrical properties have been made possible by the introduction of 2D nano- filler layers in a polymer matrix. The debonding, agglomeration, visco-elasticity, porosity, and surface contamination of the nano-fillers lead to strength and modulus limitation at the macro-and nano-grade scales. Most polymers used in the industry are anisotropic, viscoelastic and vibration dampening. In addition, viscoelastic polymers are sensitive to time, frequency, and temperature. These make the accurate and efficient design of nanocomposites resting on visco-elastic foundations and under dynamic loadings not only complicated but also of crucial importance. The design process requires extensive experimental and numerical studies. These difficulties might lead to harmful designs at worst and unnecessarily very heavy and inefficient designs at best. In view of these, the literature on the free vibration, buckling, static and dynamic bending of graphene-containing nanocomposites is wide in literature where those nanocomposites are resting on Winkler/Pasternak type foundations. However, there is no detailed study in the literature, to the best knowledge of the authors, with respect to the free vibration of functionally graded polymer composite nanoplates reinforced with graphene nano-platelets and resting on viscoelastic foundations.

This article's goal is to close this research gap. The novelty of this work lies in the comprehensive analysis of how viscoelastic foundation influence the dynamic behavior of plates. By exploring these variations, we aim to provide a deeper understanding of the mechanics involved and propose new methodologies for their calculation. This study expands on a first-order simple shear deformation theory (FSDT) that was created by Nguyen *et al*. (2019) to study the dynamic behavior of GNP-reinforced FG polymer composite nanoplates. Four distinct GNP distributions are thought to exist inside the matrix. The Halpin-Tsai model and the rule of mixture are used to calculate the effective material properties. The governing equations are derived using the Hamilton's principle.

We also analyze the effects of some important components on the dynamic, including the weight fraction of GNPs, the dimensionless geometric parameters, and the factors associated with the viscoelastic foundation.

2. Fundamental formulations

As shown in Fig. 1, the FG polymer composite nanoplate has dimensions of a, b, and h and is composed of N_L layers with thickness h = h/N_L. According to Fig. 2, there are four different distributions that designate GNPs as filler inside each layer. A pattern 2 distribution has the biggest weight fraction of GNPs in the center of the nanoplate.

According to the Halpin-Tsai model, Young's modulus of the nanoplate is calculated as follows (Affdl and Kardos 1976, She 2020).

$$E_c^{(k)} = \frac{3}{8}\frac{\xi_L \eta_L V_{GNP}^{(k)}}{\eta_L V_{GNP}^{(k)}} E_m + \frac{5}{8}\frac{1-\xi_w \eta_w V_{GNP}^{(k)}}{\eta_L V_{GNP}^{(k)}} E_m \tag{1}$$

Young's modulus of the polymeric matrix is represented here by E_m. The volume fraction of the GNP s is $V_{GNP}^{(k)}$. The parameters η_L, η_w are represented as:

$$\eta_L = \frac{\frac{E_{Gnp}}{Em} + 1}{\frac{E_{Gnp}}{Em} + \xi_L} \tag{2}$$

$$\eta_w = \frac{\frac{E_{Gnp}}{Em} - 1}{\frac{E_{Gnp}}{Em} - \xi_w} \tag{3}$$

where the size and shape of the GNP nanofillers determine ξ_L and ξ_w as shown below:

$$\xi_L = 2\frac{l_{Gnp}}{h_{Gnp}} \tag{4}$$

$$\xi_w = 2\frac{w_{Gnp}}{h_{Gnp}} \tag{5}$$

The average length, Width, and thickness of the GNPs are represented by l_{Gnp}, w_{Gnp}, h_{Gnp} respectively. In addition, the volume fraction $V_{GNP}^{(k)}$ in Eq. (1) is defined as follows

$$V_{GNP}^{(k)} = \frac{g_{Gnp}^{(k)}}{g_{Gnp}^{(k)} + \left(\frac{\rho_{Gnp}}{\rho_m}\right)\left(1 - g_{Gnp}^{(k)}\right)} \tag{6}$$

The weight fraction of the GNP polymer nanocomposite is symbolized by $g_{gnp}^{(k)}$.

The effective density and Poisson's ratio for the *k*-layer is de-fined as follows

$$\rho_c^{(k)} = \rho_{Gnp}\left(\frac{g_{Gnp}^{(k)}}{g_{Gnp}^{(k)} + \left(\frac{\rho_{Gnp}}{\rho_m}\right)\left(1 + g_{Gnp}^{(k)}\right)}\right) + \rho_m\left(\frac{g_{Gnp}^{(k)}}{g_{Gnp}^{(k)} + \left(\frac{\rho_{Gnp}}{\rho_m}\right)\left(1 + g_{Gnp}^{(k)}\right)}\right) \tag{7}$$

$$\nu_c^{(k)} = \nu_{Gnp}\left(\frac{g_{Gnp}^{(k)}}{g_{Gnp}^{(k)} + \left(\frac{\rho_{Gnp}}{\rho_m}\right)\left(1 - g_{Gnp}^{(k)}\right)}\right) + \nu_m\left(\frac{g_{Gnp}^{(k)}}{g_{Gnp}^{(k)} + \left(\frac{\rho_{Gnp}}{\rho_m}\right)\left(1 - g_{Gnp}^{(k)}\right)}\right) \tag{8}$$

ν_{Gnp}, ν_m are the Poisson's ratios of GNPs and polymer matrix, respectively. Here, we look at four different types of GNP distribution with:

$$g_{gnp}^{(k)} = \begin{cases} g_{gnp}^{*} & \text{Pattern 1} \\ \dfrac{4g_{Gnp}^{*}\left(\frac{N_L+1}{2} - \left|k - \frac{N_L+1}{2}\right|\right)}{(2+N_L)} & \text{Pattern2} \\ \dfrac{4g_{Gnp}^{*}\left(\frac{1}{2} - \left|k - \frac{N_L+1}{2}\right|\right)}{(2+N_L)} & \text{Pattern3} \\ \dfrac{2kg_{Gnp}^{*}}{(N_L+1)} & \text{Pattern4} \end{cases} \tag{9}$$

g_{Gnp}^{*} being the GNPs' weight percentage.

2.1 Refined FSDT kinematic

The present FSDT reduce the number of unknowns to four like described in the reference (Nguyen *et al*. 2019) the displacement field is given as follows:

$$\begin{aligned} u(x,y,z,t) &= u_0(x,y,t) - z\frac{\partial w_b}{\partial x} \\ v(x,y,z,t) &= v_0(x,y,t) - z\frac{\partial w_b}{\partial y} \\ w(x,y,z,t) &= w_b(x,y,t) + w_s(x,y,t) \end{aligned} \tag{10}$$

w_b and w_s denotes the bending and shear components of the transverse displacement.

The linear strain components associated with the refined FSDT displacement field are given by:

$$\begin{Bmatrix} \varepsilon_x \\ \varepsilon_y \\ \gamma_{xy} \end{Bmatrix} = \begin{Bmatrix} \varepsilon_x^0 \\ \varepsilon_y^0 \\ \gamma_{xy}^0 \end{Bmatrix} + z\begin{Bmatrix} k_x^b \\ k_y^b \\ k_{xy}^b \end{Bmatrix} \begin{Bmatrix} \gamma_{yz} \\ \gamma_{xz} \end{Bmatrix} = \begin{Bmatrix} \gamma_{yz}^0 \\ \gamma_{xz}^0 \end{Bmatrix} \tag{11}$$

$$\begin{Bmatrix} \varepsilon_x^0 \\ \varepsilon_y^0 \\ \gamma_{xy}^0 \end{Bmatrix} = \begin{Bmatrix} \dfrac{\partial u_0}{\partial x} \\ \dfrac{\partial v_0}{\partial x} \\ \dfrac{\partial u_0}{\partial y} + \dfrac{\partial v_0}{\partial x} \end{Bmatrix} \begin{Bmatrix} k_x^b \\ k_y^b \\ k_{xy}^b \end{Bmatrix} = \begin{Bmatrix} -\frac{\partial^2 w_b}{\partial x^2} \\ -\frac{\partial^2 w_b}{\partial y^2} \\ -2\frac{\partial^2 w_b}{\partial x\,\partial y} \end{Bmatrix} \tag{12}$$

$$\begin{Bmatrix} \gamma_{yz}^0 \\ \gamma_{xz}^0 \end{Bmatrix} = \begin{Bmatrix} \dfrac{\partial w_s}{\partial y} \\ \dfrac{\partial w_s}{\partial x} \end{Bmatrix}$$

In this work, to create the simple FSDT, the shear distributed function hypothesis is carried out. The shear strains vector then becomes:

$$\begin{Bmatrix} \gamma^c{}_{yz} \\ \gamma^c{}_{xz} \end{Bmatrix} = g(z)\begin{Bmatrix} \gamma_{yz}^0 \\ \gamma_{xz}^0 \end{Bmatrix} \tag{13}$$

where $g(z)$ is the function that describes how the transverse shear strains are distributed throughout the thickness of the plate (Nguyen *et al*. 2019):

$$g(z) = \frac{5}{4}cos\left(\frac{\pi z}{h}\right) \tag{14}$$

2.2 Constitutive relations and equations of Motion

The constitutive relations can be written as:

$$(1 - \mu^2\nabla^2)\begin{Bmatrix} \sigma_x \\ \sigma_y \\ \tau_{yz} \\ \tau_{xz} \\ \tau_{xy} \end{Bmatrix}^{(k)} = \begin{bmatrix} Q_{11}^{(k)} & Q_{12}^{(k)} & 0 & 0 & 0 \\ Q_{12}^{(k)} & Q_{22}^{(k)} & 0 & 0 & 0 \\ 0 & 0 & Q_{44}^{(k)} & 0 & 0 \\ 0 & 0 & 0 & Q_{55}^{(k)} & 0 \\ 0 & 0 & 0 & 0 & Q_{66}^{(k)} \end{bmatrix} \begin{Bmatrix} \varepsilon_x \\ \varepsilon_y \\ \gamma_{yz} \\ \gamma_{xz} \\ \gamma_{xy} \end{Bmatrix}^{(k)} \tag{15}$$

here

$$\begin{aligned} Q_{11}^{(k)} = Q_{22}^{(k)} &= \frac{E_c^{(k)}}{1 - \left(\nu_c^{(k)}\right)^2}; \\ Q_{12}^{(k)} = Q_{21}^{(k)} &= \nu_c^{(k)} Q_{11}^{(k)}; \\ Q_{44}^{(k)} = Q_{55}^{(k)} = Q_{55}^{(k)} &= \frac{E_c^{(k)}}{2\left(1 + \nu_c^{(k)}\right)} \end{aligned} \tag{16}$$

where ν represents the nonlocal parameter to describe the stiffness-softening.

The governing equations of motion in the following

method are derived using the Hamilton principle (Shanab *et al*. 2023, Rajendran *et al*. 2024).

$$\int_{t_1}^{t_2}(\delta\, U - \delta\, K + \delta\, V)dt = 0 \tag{17}$$

where the terms *U*, *K* and *V* stand for, respectively, strain energy, kinetic energy, and the external energy brought on by the foundation's reaction force.

Equations of motion can be obtained by substituting Eq. (11) into Eq. (15) and applying Eqs. (17) and (10), as follows:

$$\begin{aligned} &A_{11}d_{11}u_0 + A_{66}d_{22}u_0 + (A_{12}+A_{66})d_{12}v_0 - \\ &B_{11}d_{111}w_b - (B_{12}+2B_{66})d_{122}w_b = \\ &(1-\mu^2\nabla^2)\big(I_0\ddot{u}_0 - I_1d_1\ddot{w}_b\big), \end{aligned} \tag{18a}$$

$$\begin{aligned} &A_{22}d_{22}v_0 + A_{66}d_{11}v_0 + (A_{12}+A_{66})d_{12}u_0 - \\ &B_{22}d_{222}w_b - (B_{12}+2B_{66})d_{112}w_b = \\ &(1-\mu^2\nabla^2)(I_0\ddot{v}_0 - I_1d_2\ddot{w}_b), \end{aligned} \tag{18b}$$

$$\begin{aligned} &B_{11}d_{111}u_0 + (B_{12}+2B_{66})d_{122}u_0 + \\ &(B_{12}+2B_{66})d_{112}v_0 + B_{22}d_{222}v_0 - \\ &D_{11}d_{1111}w_b - 2(2D_{66}+D_{12})d_{1122}w_b - \\ &D_{22}d_{2222}w_b + (1-\mu^2\nabla^2)\begin{pmatrix}-k_1(w_b+w_s)+\\ k_2\nabla^2(w_b+w_s)-\\ c_t\dfrac{\partial}{\partial t}(w_b+w_s)\end{pmatrix} = \\ &(1-\mu^2\nabla^2)\begin{pmatrix}I_0(\ddot{w}_b+\ddot{w}_s)+\\ I_1(d_1\ddot{u}_0+d_2\ddot{v}_0)\\ -I_2(d_{11}\ddot{w}_b+d_{22}\ddot{w}_b)\end{pmatrix} \end{aligned} \tag{18c}$$

$$\begin{aligned} &A_{44}^s d_{22}w_s + A_{55}^s d_{11}w_s + (1-\mu^2\nabla^2) \\ &\begin{pmatrix}-k_1(w_b+w_s)+k_2\nabla^2(w_b+w_s)-\\ c_t\dfrac{\partial}{\partial t}(w_b+w_s)\end{pmatrix} = \\ &(1-\mu^2\nabla^2)\begin{pmatrix}I_0(\ddot{w}_b+\ddot{w}_s)+\\ J_1(d_1\ddot{u}_0+d_2\ddot{v}_0)\\ -J_2(d_{11}\ddot{w}_b+d_{22}\ddot{w}_b)\end{pmatrix} \end{aligned} \tag{18d}$$

k_1 represents Winkler parameter, while k_2 and c_t are the shear layer foundation stiffness and viscosity parameter, respectively.

Where d_{ij}, d_{ijl} and d_{ijlm} are the following differential operators:

$$\begin{aligned} &d_{ij} = \frac{\partial^2}{\partial x_i \partial x_j}, d_{ijl} = \frac{\partial^3}{\partial x_i \partial x_j \partial x_l} \\ &d_{ijlm} = \frac{\partial^4}{\partial x_i \partial x_j \partial x_l \partial x_m}, d_i = \frac{\partial}{\partial x_i}(i,j,l,m = 1,2) \end{aligned} \tag{19}$$

And stiffness components are given as:

$$(A_{ij}, B_{ij}, D_{ij}) = \sum_{k=1}^{N_l}\int_{z(k)}^{z(k+z)} Q^k{}_{ij}(1, z, z^2)dz\,, \quad (i,j = 1,2,6), \tag{20}$$

The inertias are also defined as:

$$(I_0, I_1, I_2) = \sum_{k=1}^{N_l}\int_{z(k)}^{z(k+z)}(1, z, z^2)dz\rho_c^{(k)} \tag{21}$$

3. Analytical solutions

The solution process for a FG composite nanoplate with simply supported boundary conditions is presented in this section. In accordance with Navier's technique (Esen *et al*. 2023, Abdelrahman *et al*. 2024, Draiche *et al*. 2024, Djedid *et al*. 2024, Madenci *et al*. 2024 a, b), we define the displacement field using a trigonometric series along the x and y directions.

$$\begin{Bmatrix}u_0\\ v_0\\ w_b\\ w_s\end{Bmatrix} = \sum_{m=1}^{\infty}\sum_{n=1}^{\infty}\begin{Bmatrix}U_{mn}e^{i\omega\, t}\cos(\lambda\, x)\sin(\mu\, y)\\ V_{mn}e^{i\omega\, t}\sin(\lambda\, x)\cos(\mu\, y)\\ W_{bmn}e^{i\omega\, t}\sin(\lambda\, x)\sin(\mu\, y)\\ W_{smn}e^{i\omega\, t}\sin(\lambda\, x)\sin(\mu\, y)\end{Bmatrix} \tag{22}$$

where U_{mn}, V_{mn}, W_{bmn} and W_{smn} are arbitrary parameters to be determined, ω is the eigenfrequency associated with (m,n) the eigenmode, and $\lambda = m\pi/a$ and $\mu = n\pi/b$.

Substituting the Eq. (20) into equations of motion (16a)-(16d), The frequency equation shown below is discovered:

$$\left(\begin{bmatrix}a_{11}&a_{12}&a_{13}&a_{14}\\ a_{12}&a_{22}&a_{23}&a_{24}\\ a_{13}&a_{23}&a_{33}&a_{34}\\ a_{14}&a_{24}&a_{34}&a_{44}\end{bmatrix} - \omega^2\alpha\begin{bmatrix}m_{11}&0&m_{13}&m_{14}\\ 0&m_{22}&m_{23}&m_{24}\\ m_{13}&m_{23}&m_{33}&m_{34}\\ m_{14}&m_{24}&m_{34}&m_{44}\end{bmatrix}\right) = \begin{Bmatrix}0\\0\\0\\0\end{Bmatrix} \tag{23}$$

In which:

$$\begin{aligned} a_{11} &= -\lambda^2 A_{11} - \mu^2 A_{66} \\ a_{12} &= -\lambda\mu(A_{12}+A_{66}) \\ a_{13} &= \lambda[\lambda^2 B_{11} + (B_{12}+2B_{66})\mu^2] \\ a_{14} &= 0 \\ a_{22} &= -\lambda^2 A_{66} - \mu^2 A_{22} \\ a_{23} &= \mu[\mu^2 B_{22} + (B_{12}+2B_{66})\lambda^2] \\ a_{24} &= 0 \\ a_{33} &= -[D_{11}\lambda^4 + 2(D_{12}+2D_{66})\lambda^2\mu^2 + D_{22}\mu^4] - \\ &\alpha[k_1 + (\mu^2+\lambda^2)k_1 + c_t] \\ a_{34} &= 0 \\ a_{44} &= -[A_{55}^s\lambda^2 + \mu^2 A_{44}^s] - \alpha \\ &[k_1 + (\mu^2+\lambda^2)k_1 + c_t] \\ m_{11} &= I_1 \\ m_{12} &= 0 \\ m_{13} &= -I_2\lambda \\ m_{14} &= 0 \\ m_{22} &= I_1 \\ m_{23} &= -I_2\mu \\ m_{24} &= 0 \\ m_{33} &= I_1 + I_3(\mu^2+\lambda^2) \\ m_{34} &= I_1 \\ m_{44} &= I_1 \\ \alpha &= 1 + \mu(\mu^2+\lambda^2) \end{aligned} \tag{24}$$

4. Numerical results

Here, the numerical solution to the issue is set out in

Table 1 Comparative evaluation of the natural frequencies for different modes and patterns.($k_1 = 5 \times 10^{15} N/m^3; k_2 = 4N/m$)

patterns	theory	(*m*, *n*)					
		(1,1)	(2,1)	(2,2)	(3,1)	(3,2)	(3,3)
Pure epoxy	Ref. (Jiao and Alavi 2018)	0.0584	0.1391	0.2132	0.2595	0.3251	0.4261
	Ref. (Aditya *et al*. 2019)	0.0584	0.1391	0.2133	0.2597	0.3254	0.4267
	present	0.0584	0.1387	0.2123	0.2582	0.3232	0.4231
Pattern 1	Ref. (Jiao and Alavi 2018)	0.1216	0.2895	0.4436	0.5400	0.6767	0.8869
	Ref. (Aditya *et al*. 2019)	0.1216	0.2896	0.4438	0.5403	0.6773	0.8881
	present	0.1214	0.2887	0.4417	0.5374	0.6727	0.8806
Pattern 2	Ref. (Jiao and Alavi 2018)	0.1020	0.2456	0.3796	0.4645	0.5860	0.7755
	Ref. (Aditya *et al*. 2019)	0.1023	0.2471	0.3830	0.4694	0.5934	0.7877
	present	0.1022	0.2467	0.3822	0.4682	0.5917	0.7849
Pattern 3	Ref. (Jiao and Alavi 2018)	0.1378	0.3249	0.4939	0.5984	0.7454	0.9690
	Ref. (Aditya *et al*. 2019)	0.1365	0.3183	0.4798	0.5787	0.7168	0.9251
	present	0.1365	0.3186	0.4803	0.5793	0.7174	0.9252
Pattern 4	Ref. (Jiao and Alavi 2018)	0.1118	0.2673	0.4110	0.5013	0.6299	0.8287
	Ref. (Aditya *et al*. 2019)	0.1118	0.2671	0.4107	0.5009	0.6294	0.8282
	present	0.1118	0.2667	0.4095	0.4992	0.6267	0.8236

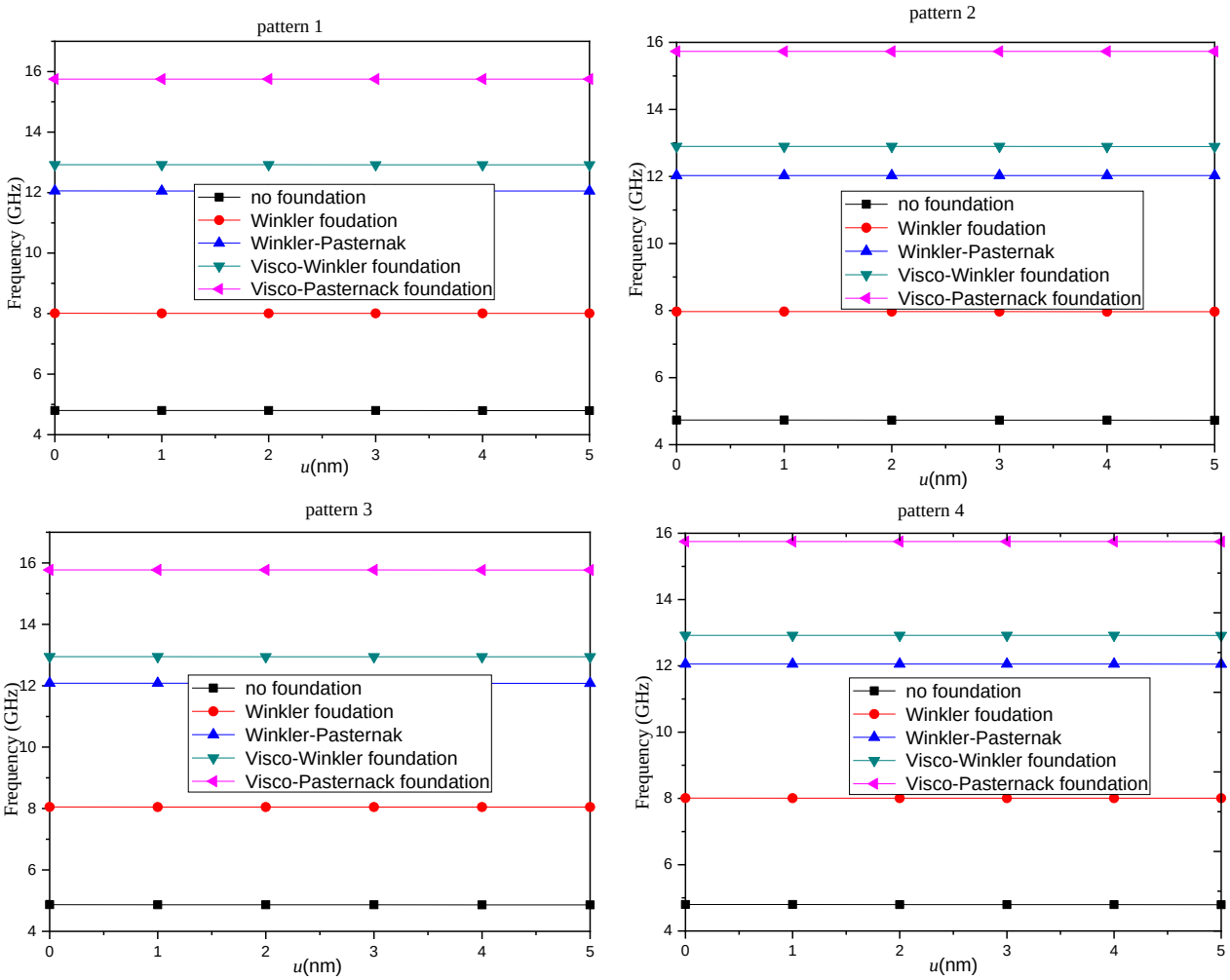

Fig. 3 first natural frequency vs. nonlocal parameter μ for different foundations

Table 2 Natural frequencies (in GHz) of the nanoplate for different weight fractions g^*_{GNP} and nonlocal parameter μ

μ	(i,j)	theory	$g^*_{GNP}\left(\frac{0}{0}\right)$				
			0.2	0.4	0.6	0.8	1
0	(1,1)	Ref. (Arefi *et al*. 2018)	4.6717	4.7234	4.7748	4.8259	4.8767
		present	4.6648	4.7159	4.7667	4.8173	4.8675
	(2,2)	Ref. (Arefi *et al*. 2018)	17.0375	17.2153	17.3920	17.5676	17.7422
		present	16.9581	17.1338	17.3085	11.4373	17.6549
	(3,3)	Ref. (Arefi *et al*. 2018)	34.0683	34.4015	34.7325	35.0612	35.3879
		present	33.7765	34.1053	34.4321	34.7570	35.0800
1	(1,1)	Ref. (Arefi *et al*. 2018)	4.6705	4.7222	4.7736	4.8247	4.8755
		present	4.6636	4.7147	4.7656	4.8161	4.8664
	(2,2)	Ref. (Arefi *et al*. 2018)	17.0207	17.1984	17.3749	17.5503	17.7247
		present	16.9414	17.1169	17.2915	17.4649	17.6375
	(3,3)	Ref. (Arefi *et al*. 2018)	33.9929	34.3254	34.6556	34.9836	35.3096
		present	33.7017	34.0298	34.3559	34.6801	35.0024
2	(1,1)	Ref. (Arefi *et al*. 2018)	4.6670	4. 7187	4.7701	4.8211	4.8719
		present	4.6625	4.7136	4.7644	4.8149	4.8651
	(2,2)	Ref. (Arefi *et al*. 2018)	16.9706	17.1478	17.3238	17.4987	17.6726
		present	16.9247	17.1001	17.2744	17.4478	17.6201
	(3,3)	Ref. (Arefi *et al*. 2018)	33.7696	34.1000	34.4280	34.7539	35.0777
		present	33.6275	33.9548	34.2802	34.6036	34.9255
3	(1,1)	Ref. (Arefi *et al*. 2018)	4.6613	4.7129	4.7642	4.8152	4.8659
		present	4.6613	4.7124	4.7632	4.8137	4.8639
	(2,2)	Ref. (Arefi *et al*. 2018)	16.8881	17.0644	17.2396	17.4136	17.5867
		present	16.9081	17.0833	17.2575	17.4307	17.6029
	(3,3)	Ref. (Arefi *et al*. 2018)	33.4072	33.7339	34.0585	34.3808	34.7012
		present	33.5537	33.8803	34.2050	34.5277	34.8486
4	(1,1)	Ref. (Arefi *et al*. 2018)	4.6533	4. 7048	4.7560	4.8069	4.8576
		present	4.6602	4.7113	4.7620	4.8125	4.8628
	(2,2)	Ref. (Arefi *et al*. 2018)	16.7747	16.9498	17.1237	17.2966	17.4685
		present	16.8915	17.0666	17.2406	17.4136	17.5856
	(3,3)	Ref. (Arefi *et al*. 2018)	32.9187	33.2407	33.5605	33.8782	34.1938
		present	33.4804	33.8063	34.1303	34.4523	34.7725
5	(1,1)	Ref. (Arefi *et al*. 2018)	4.6431	4.6945	4.7456	4.7964	4.8469
		present	4.6590	4.7101	4.7609	4.8114	4.8616
	(2,2)	Ref. (Arefi *et al*. 2018)	16.6321	16.8057	16.9782	17.1496	17.3200
		present	16.8750	17.0499	17.2237	17.3966	17.5684
	(3,3)	Ref. (Arefi *et al*. 2018)	32.3211	32.6373	32.9513	33.2632	33.5731
		present	33.4076	33.7328	34.0560	34.3774	34.6969

terms of the composite nanoplate's natural frequencies. The numerical formulation that is herein proposed is first verified through a comparison of our findings with certain reliable hypotheses from the literature.

We investigate an FG composite nanoplate's vibrating behavior in order to achieve this goal. The natural frequencies of an FG composite plate reinforced with GNPs are listed in Table 1 for various modes and patterns. Epoxy is chosen as the polymer matrix. The plate is reinforced with GPLs with dimensions as described in the reference (Jiao and Alavi 2018). Our simplified FSDT-based results are successfully contrasted to literary predictions (Jiao and Alavi 2018), based on the conventional model where the shape function f (z) equals z, and predictions based on the two-variable sinusoidal shear deformation theory (Aditya *et al*. 2019). The pattern 3 distribution of GNPs inside the

Table 3 Natural frequencies (in GHz) of the nanoplate for different weight fractions, nonlocal parameter, foundations' damping coefficients $(10^{15}N.s/m^3)$ $(k_1 = 5 \times 10^{15}N/m^3; k_2 = 4N/m)$

μ	C_t	$g^*_{GNP}\left(\frac{0}{0}\right)$				
		0.2	0.4	0.6	0.8	1
0	0	17.5554	17.5713	17.5873	17.6034	17.6195
	1	18.1307	18.1464	18.1620	18.1777	18.1935
	5	20.2693	20.2839	20.2985	20.3132	20.3278
	10	21.6369	21.8180	21.9986	22.1787	22.3585
1	0	17.5551	17.5710	17.5870	17.6031	17.6192
	1	18.1304	18.1461	18.1617	18.1774	18.1932
	5	20.2691	20.2836	20.2982	20.3129	20.3276
	10	21.6316	21.8126	21.9932	20.3129	22.3530
2	0	17.5547	17.5707	17.5867	17.6028	17.6189
	1	18.1301	18.1458	18.1614	18.1771	18.1929
	5	20.2688	20.2834	20.2979	20.3126	20.3273
	10	21.6263	21.8073	21.9878	22.1678	22.3475
3	0	17.5545	17.5704	17.5864	17.6024	17.6186
	1	18.1298	18.1454	18.1611	18.1768	18.1926
	5	20.2686	20.2831	20.2977	20.3123	20.3270
	10	21.6209	21.8019	21.9224	22.1624	22.3420
4	0	17.5542	17.5701	17.5861	17.6021	17.6182
	1	18.1296	18.1451	18.1607	18.1765	18.1922
	5	20.2680	20.2828	20.2974	20.3120	20.3267
	10	21.6157	21.7965	21.9769	22.1569	22.3365
5	0	17.5539	17.5698	17.5858	17.6018	17.6179
	1	18.1293	18.1448	18.1604	18.1762	18.1919
	5	20.2680	20.2825	20.2971	20.3117	20.3264
	10	21.6103	21.7912	21.9715	22.1514	22.3309

matrix achieves the highest natural frequencies for FG composite materials, whereas the pattern 2 achieves the lowest values with the same concentration of GNP additives. This final design yields greater frequencies in comparison to a pure epoxy matrix, demonstrating the material's benefit from the presence of GNPs.

The improvement in plate stiffness and consequently the fundamental natural frequency by the incorporation of GNPs is particularly noteworthy, this clearly shows that the most efficient way to increase plate stiffness for noticeably higher natural frequencies is to disperse more GNP nanofillers near the top and bottom surfaces of the plate, where there is a very high normal stress, and much less content near its mid-plane, where there is a very low normal stress. This is because such a distribution may utilize high modulus GNP nanofillers most effectively, which results in the greatest increase in plate stiffness elements.

Following, we take into consideration an epoxy matrix with: Em=3GPa, V_m=0.34, and ρ_m=1200 kg/m^3.

The variation of the GNP-reinforced nanoplate's natural frequencies (measured in GHz) is shown in Table 2 for various GNP weight fractions and nonlocal parameters. The pattern 3 distribution of GNPs in the matrix, which would correspond to the highest natural frequencies, is the distribution for which the data are presented here. The nanoplate is also expected to have a total of N_L = 10 layers. According to Table 2's findings, the natural frequencies increase significantly when the weight fraction of GNPs increases. As could be expected, the nonlocal parameter has a significant impact on the structural vibrating response, with an increase in the nonlocal parameter clearly causing a drop in the structural stiffness and vibrations. Again, a good agreement in results is observed.

Tables 3 presents the natural frequencies for the plate resting on a three-parameter viscoelastic foundation with different weight fractions g^*_{gnp} and nonlocal parameter. In this table, It can be noticed the influence of the damping coefficient increase with the increase of weight fractions.

Fig. 3 shows the impact of several foundation models on the relationship between frequencies and non local parameter. When the damping coefficient increases or the Winkler or Pasternak parameters increase, the frequency also increases. Thus, the plate lying on the visco-Pasternak foundation exhibits the maximum frequency. Figures 4 illustrate the damping coefficient influence on the frequencies with the non local parameter. It is noticed that the frequencies

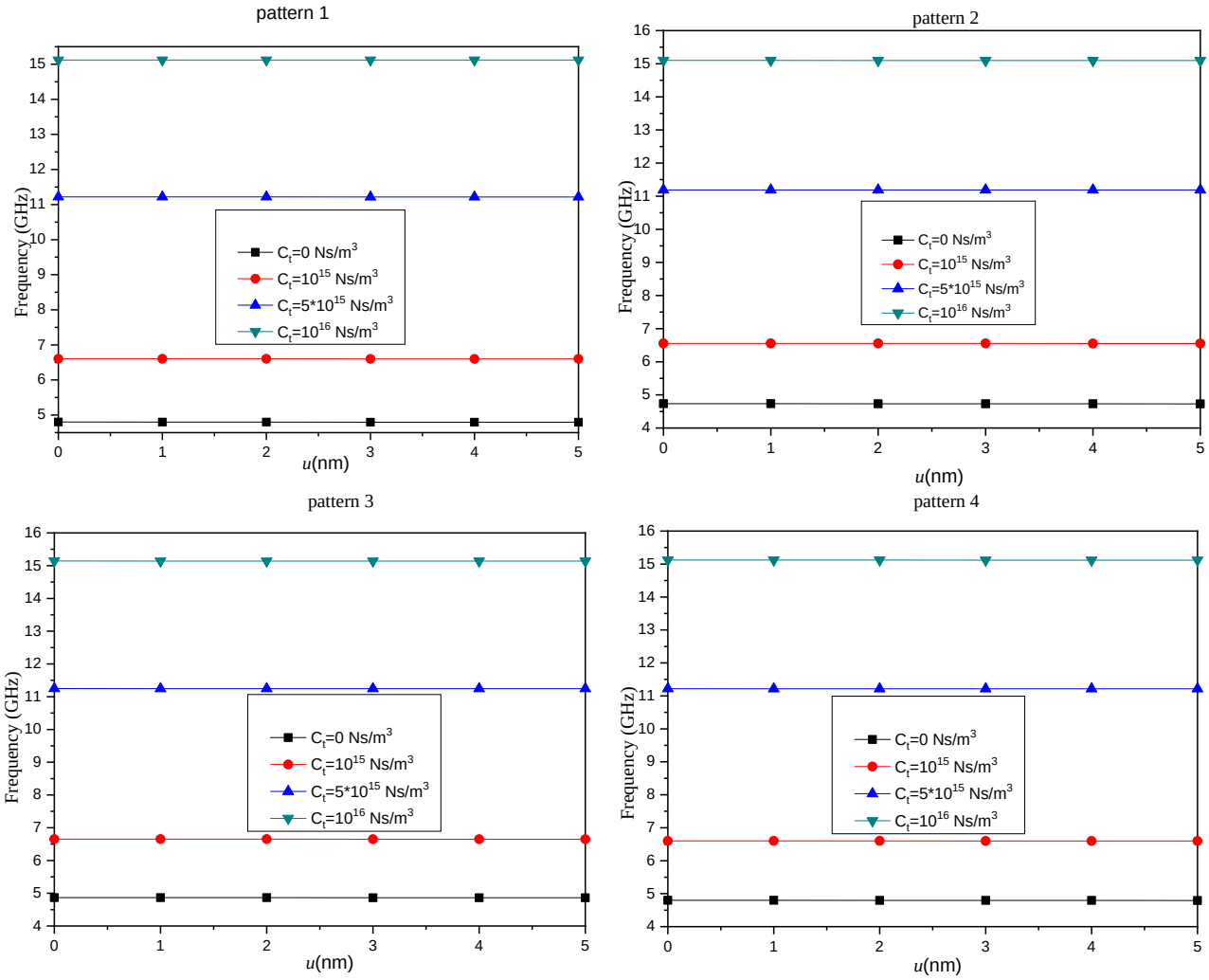

Fig. 4 Effect of the foundation's damping coefficient on the nanoplate $(k_1 = 5 \times 10^{15} N/m^3; k_2 = 4N/m;)$

increase with the increase of the damping coefficient.

The viscoelastic foundation, characterized by its unique mechanical properties, not only provides a certain degree of elastic support but also facilitates the dissipation of energy through deformation that is dependent on the passage of time. This complex interaction has a significant impact on the dynamic response exhibited by nanoplates, as it effectively modifies critical parameters such as their natural frequencies and the damping characteristics associated with their vibrational modes. The intrinsic viscoelastic properties engender a notable phase lag between the applied stress and the resulting strain, which subsequently introduces frequency-dependent damping effects that have the potential to intensify vibrations.

An additional parametric study looks into how the shape and size of GNPs affect the response in terms of the first natural frequency. For all the patterns in Fig. 5, a dimensionless length-to-thickness ratio I_{GNP}/h_{GNP} is progressively increased from 1 to 500. For length-to-width dimensionless ratios, $\frac{I_{GNP}}{w_{GNP}} = \frac{5}{3}$. The plot in Fig. 5 indicates that as I_{GNP}/h_{GNP} values grow, the first natural frequency increases accordingly.

5. Conclusions

In this research, we examine the free vibration characteristics of functionally graded (FG) composite nanoplates that are reinforced with graphene nanoplates (GNPs) and supported by a viscoelastic foundation. To address this, we integrate the nonlocal elastic theory with the four-variable first-order shear deformation theory (FSDT). Initially, we validate our proposed method against existing literature for different GNP distributions and various geometric and nonlocal parameters. Additionally, we aim to explore how factors such as the GNP dispersion distribution, nonlocal parameters, weight fraction, aspect ratio, and damping coefficient influence the free vibration response of the reinforced nanoplate.

According to the numerical analysis, the higher bending stiffness of the composite in this reinforcement mode results in pattern 3, which yields the highest natural frequency among the distributions studied. However, an increase in the value of the nonlocal parameter causes a decrease in the natural frequency of the nanoplates. Additionally, the size, shape, and weight fraction of the GNPs significantly influence the fundamental frequency of the structure. This

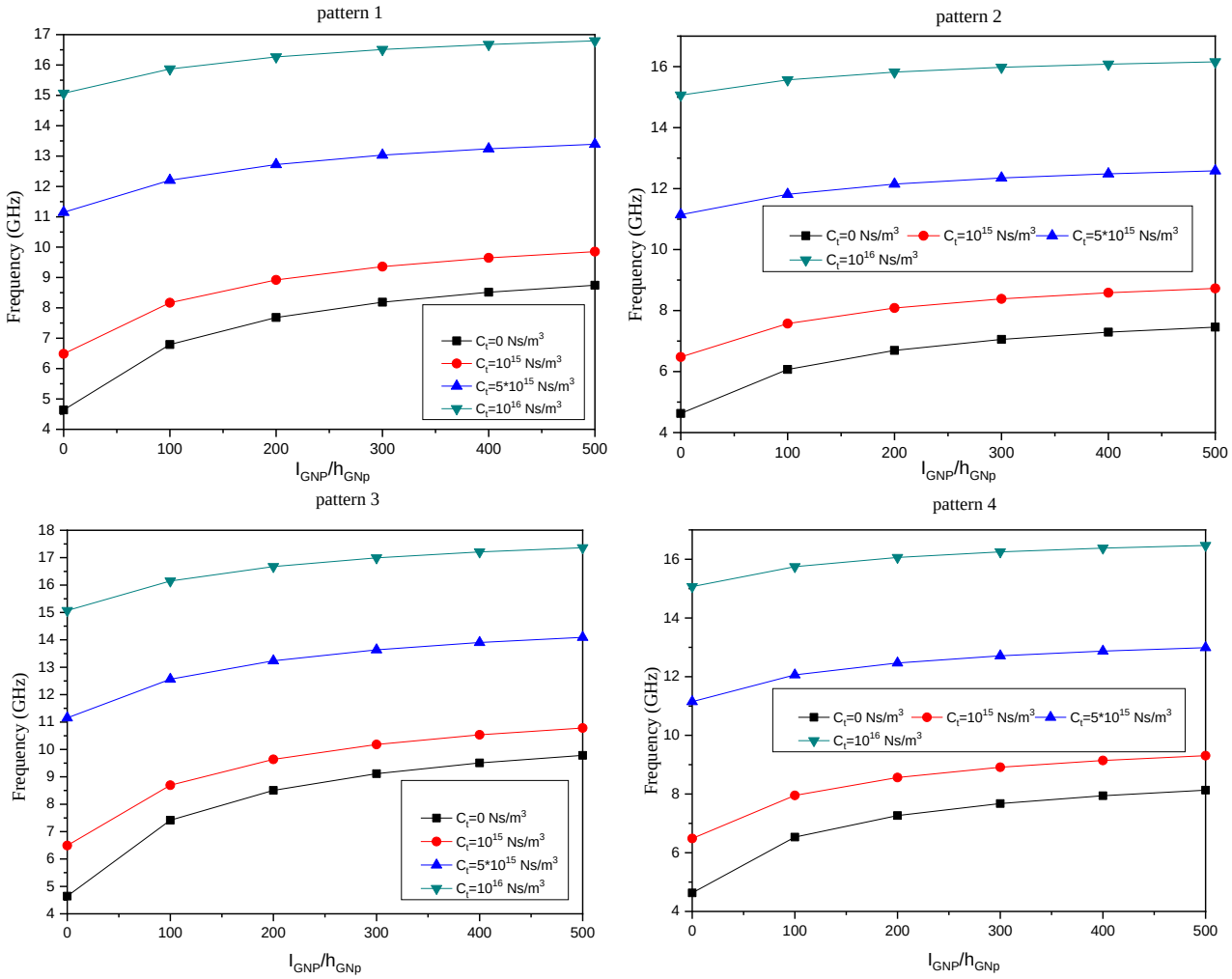

Fig. 5 Effect of the GNPs geometry and size on the first natural frequency $(k_1 = 5 \times 10^{15} N/m^3; k_2 = 4N/m; \mu = 2)$

information is valuable for researchers and designers aiming for optimization. The final focus of this paper is on the sensitivity of the response to the damping coefficient, which significantly increases the frequency of thecomposite structure with greater fundamental stiffness. The type of material studied can be extended and applied to other structures subjected to various external loadings as referenced in (Ahmed *et al.* 2019, Avcar 2019, Madenci 2019, Mehar and Panda 2019, Al-Basyouni *et al.* 2020, Abed and Majeed 2020, Asrari *et al.* 2020, Yahea and Majeed 2021, Madenci and Özütok 2020, Mehar *et al.* 2020, Yaylaci 2022, Moradi *et al.* 2023, Eltaher *et al.* 2024). In addition, combining experimental and theoretical analyses can provide valuable insights into the behavior of plates in various engineering applications. This approach not only enhances the understanding of the mechanical properties of the materials used but also aids in the design of more robust structures (Hakeem *et al.* 2024, Madenci *et al.* 2023).

Acknowledgement

This project was funded by the Deanship of Scientific Research (DSR) at King Abdulaziz University, Jeddah, Saudi Arabia, under grant no. (GPIP: 1442-156-2024). The authors, therefore, acknowledge with thanks DSR for its technical and financial support.

References

Abdelrahman, A.A., Esen, I., Tharwan, M.Y., Assie, A. and Eltaher, M.A. (2024), "On vibrations of functionally graded carbon nanotube (FGCNT) nanoplates under moving load", *Adv. Nano Res.*, **16**(4), 395-412. https://doi.org/10.12989/ANR.2024.16.4.395

Abed Z.A.K. and Majeed, W.I. (2020), "Effect of boundary conditions on harmonic response of laminated plates", *Compos. Mater. Eng.*, **2**(2), 125-140. https://doi.org/10.12989/cme.2020.2.2.125.

Aditya, N.D., Ben, Z.T., Polit, O., Pradyumna B. and Ganapathi, M. (2019), "Large amplitude free flexural vibrations of functionally graded graphene platelets reinforced porous composite curved beams using finite element based on trigonometric shear deformation theory", *Int. J. Nonlinear. Mech.*, **116**, 302-317. https://doi.org/10.1016/j.ijnonlinmec.2019.07.010.

Affdl, J.H. and Kardos, J.L. (1976), "The Halpin-Tsai equations: a review", *Polym. Eng. Sci.*, **16**(5), 344-352. https://doi.org/10.1002/pen.760160512

Afshari, H. and Adab, N. (2022), "Size-dependent buckling and

vibration analyses of GNP reinforced microplates based on the quasi-3D sinusoidal shear deformation theory", *Mech. Based Des. Struct. Machin.*, **50**(1), 184-205. https://doi.org/10.1080/15397734.2020.1713158

Ahmed, R.A., Fenjan, R.M., Faleh, N.M. (2019), "Analyzing post-buckling behavior of continuously graded FG nanobeams with geometrical imperfections", *Geomech. Eng.*, **17**(2), 175-180. https://doi.org/10.12989/gae.2019.17.2.175.

Al Mahmud, H., Radue, M.S., Chinkanjanarot, S. and Odegard, G. M. (2021), "Multiscale modeling of epoxy-based nanocomposites reinforced with functionalized and non functionalized graphene nanoplatelets", *Polymers*, **13**(12), 1958. https://doi.org/10.3390/polym13121958

Al-Basyouni, K.S., Ghandourah, E., Mostafa, H.M. and Algarni, A. (2020), "Effect of the rotation on the thermal stress wave propagation in non-homogeneous viscoelastic body", *Geomech. Eng.*, **21**(1), 1-9. https://doi.org/10.12989/GAE.2020.21.1.001.

Arefi, M., Firouzeh, S., Bidgoli, E.M.R. and Civalek, Ö. (2020), "Analysis of porous micro-plates reinforced with FG-GNPs based on Reddy plate theory", *Compos. Struct.*, **247**, 112391. https://doi.org/10.1016/j.compstruct.2020.112391

Asrari, R., Ebrahimi, F. and Kheirikhah, M.M. (2020), "On post-buckling characteristics of functionally graded smart magneto-electro-elastic nanoscale shells", *Adv. Nano Res.*, **9**(1), 33-45. https://doi.org/10.12989/ANR.2020.9.1.033

Avcar, M. (2019), "Free vibration of imperfect sigmoid and power law functionally graded beams", *Steel Compos. Struct.*, **30**(6), 603-615. https://doi.org/10.12989/SCS.2019.30.6.603

Djedid, I.K., Yahia, S.A., Draiche, K., Madenci, E., Benrahou, K. H. and Tounsi, A. (2024), "A new four-unknown equivalent single layer refined plate model for buckling analysis of functionally graded rectangular plates", *Struct. Eng. Mech.*, **90**(5), 517-530. https://doi.org/10.12989/sem.2024.90.5.517

Dong, M., Zhang, H., Tzounis, L., Santagiuliana, G., Bilotti, E. and Papageorgiou, D.G. (2021), "Multifunctional epoxy nanocomposites reinforced by two-dimensional materials: A review", *Carbon*, **185**, 57-81. https://doi.org/10.1016/j.carbon.2021.09.009

Draiche, K., Madenci, E., Djedid, I.K. and Tounsi, A. (2024), "An optimized 2D kinematic model for flexure and free vibration analysis of functionally graded plates", *Steel Compos. Struct.*, **53**(4), 491-508. https://doi.org/10.12989/scs.2024.53.4.491

Ebrahimi, F., Hashemabadi, D., Habibi, M. and Safarpour, H. (2020), "Thermal buckling and forced vibration characteristics of a porous GNP reinforced nanocomposite cylindrical shell", *Microsyst. Technol.*, **26**, 461-473. https://doi.org/10.1007/s00542-019-04542-9

Eltaher, M.A., Esen, I., Abdelrahman, A.A. and Abdraboh, A.M. (2024), "Dynamic response of FG carbon nanotubes nanoplates embedded in elastic media under moving point load", *Adv. Nano Res.*, **17**(3), 257-274. https://doi.org/10.12989/ANR.2024.17.3.257

Esen, I., Alazwari, M.A., Almitani, K.H., Eltaher, M.A. and Abdelrahman, A. (2023), "Dynamic vibration response of functionally graded porous nanoplates in thermal and magnetic fields under moving load", *Adv. Nano Res.*, **14**(5), 475-493. https://doi.org/10.12989/ANR.2023.14.5.475

Ghasemi, H., Mohammadi, Y. and Ebrahimi, F. (2023), "Free vibration analysis of FG-GPL and FG-CNT hybrid laminated nano composite truncated conical shells using systematic differential quadrature method", *ZAMM J. Appl. Math. Mech.*, **103**(11), e202300280. https://doi.org/10.1002/zamm.202300280

Hakeem, I.Y., Madenci, E., Bahrami, A., Özkılıç, Y.O., Rizal Muhammad Asyraf, M., Tawfik, T.A. and Fayed, S. (2024), "Nonlocal theoretical inquiry into pultruded GFRP plate dynamics: Integrating experimental and numerical analyses", *J. Eng. Fibers Fabrics*, **19**, 15589250241246072. https://doi.org/10.1177/15589250241246072

Jayakumari, B.Y., Swaminathan, E.N. and Partheeban, P. (2024), "Sustainable construction material using nanosilica and multi-walled carbon nanotubes in cement concrete", *Adv. Nano Res.*, **16**(5), 459-472. https://doi.org/10.12989/anr.2024.16.5.459

Jiao, P. and Alavi, A.H. (2018), "Buckling analysis of graphene-reinforced mechanical metamaterial beams with periodic webbing patterns", *Int. J. Eng. Sci.*, **131**, 1-18. https://doi.org/10.1016/j.ijengsci.2018.06.005

Liu, D. (2020), "Free vibration of functionally graded graphene platelets reinforced magnetic nanocomposite beams resting on elastic foundation", *Nanomaterials*, **10**(11), 2193. https://doi.org/10.3390/nano10112193

Liu, D., Su, J., Zhao, L. and Shen, X. (2024), "State-space formulation for buckling and free vibration of axially functionally graded graphene reinforced nanocomposite microbeam under axially varying loads", *Materials*, **17**(6), 1296. https://doi.org/10.3390/ma17061296

Liu, M., Cataldi, P., Young, R.J., Papageorgiou, D.G. and Kinloch, I.A. (2021), "High-performance fluoroelastomer-graphene nanocomposites for advanced sealing applications", *Compos. Sci. Technol.*, **202**, 108592. https://doi.org/10.1016/j.compscitech.2020.108592

Madenci, E. (2019), "A refined functional and mixed formulation to static analyses of fgm beams", *Struct. Eng. Mech.*, **69**(4), 427-437. https://doi.org/10.12989/sem.2019.69.4.427.

Madenci, E. and Özütok, A. (2020), "Variational approximate for high order bending analysis of laminated composite plates", *Struct. Eng. Mech.*, **73**(1), 97-108. https://doi.org/10.12989/sem.2020.73.1.097.

Madenci, E., Gulcu, S. and Draiche, K. (2024b), "Analytical nonlocal elasticity solution and ANN approximate for free vibration response of layered carbon nanotube reinforced composite beams", *Adv. Nano Res.*, **16**(3), 251-263. https://doi.org/10.12989/anr.2024.16.3.251

Madenci, E., Özkılıç, Y.O., Bahrami, A., Aksoylu, C., Asyraf, M.R.M., Hakeem, I.Y., ... and Fayed, S. (2024a), "Experimental investigation and analytical verification of buckling of functionally graded carbon nanotube-reinforced sandwich beams", *Heliyon*, **10**(8). https://doi.org/10.1016/j.heliyon.2024.e28388

Madenci, E., Ozkilic, Y.O., Hakamy, A. and Tounsi, A. (2023), "Experimental tensile test and micro-mechanic investigation on carbon nanotube reinforced carbon fiber composite beams", *Adv. Nano Res.*, **14**(5), 443-450. https://doi.org/10.12989/anr.2023.14.5.443

Mehar, K. and Panda, S.K. (2019), "Multiscale modeling approach for thermal buckling analysis of nanocomposite curved structure", *Adv. Nano Res.*, **7**(3), 181-190. https://doi.org/10.12989/ANR.2019.7.3.181.

Mehar, K., Panda, S.K., Yuvarajan, D. and Gautam, C. (2019), "Numerical buckling analysis of graded CNT-reinforced composite sandwich shell structure under thermal loading", *Compos. Struct.*, S0263822318344763. https://doi.org/10.1016/j.compstruct.2019.03.002.

Mohammad-Rezaei Bidgoli, E. and Arefi, M. (2021), "Free vibration analysis of micro plate reinforced with functionally graded graphene nanoplatelets based on modified strain-gradient formulation", *J. Sandw. Struct. Mater.*, **23**(2), 436-472. https://doi.org/10.1177/1099636219839302

Moradi, Z., Ebrahimi, F. and Davoudi, M. (2023), "Vibration control, energy harvesting and forced vibration of the piezoelectric NEMS via paradox-free local/nonlocal theory", *Adv. Nano Res.*, **14**(4), 335-353. https://doi.org/10.12989/ANR.2023.14.4.335

Nguyen, H.N., Hong, T.T., Vinh, P.V., Quang, N.D. and Thom, D.V. (2019), "A refined simple first-order shear deformation theory for static bending and free vibration analysis of advanced

composite plates", *Materials*, **12**(15), 2385. https://doi.org/10.3390/ma12152385.

Rajendran, S., Loganathan, R., Yaylaci, M., Yaylaci, E.U. and Ozdemir, M.E. (2024), "Vibration of piezo-magneto-thermoelastic FG nanobeam submerged in fluid with variable nonlocal parameter", *Adv. Nano Res.*, **16**(5), 489-500. https://doi.org/10.12989/ANR.2024.16.5.489

Sahmani, S. and Aghdam, M.M. (2017), "Nonlocal strain gradient beam model for nonlinear vibration of prebuckled and postbuckled multilayer functionally graded GPLRC nanobeams", *Compos. Struct.*, **179**, 77-88. https://doi.org/10.1016/j.compstruct.2017.07.064

Shanab, R.A., Mohamed, N.A., Eltaher, M.A. and Abdelrahman, A.A. (2023), "Dynamic characteristics of viscoelastic nanobeams including cutouts", *Adv. Nano Res.*, **14**(1), 45-65. https://doi.org/10.12989/ANR.2023.14.1.045

She, G.L. (2020), "Wave propagation of FG polymer composite nanoplates reinforced with GNPs", *Steel Compos. Struct*, **37**(1), 27-35. https://doi.org/10.12989/scs.2020.37.1.027

She, G.L., Liu, H.B. and Karami, B. (2021), "Resonance analysis of composite curved microbeams reinforced with graphene nanoplatelets", *Thin Wall. Struct.*, **160**, 107407. https://doi.org/10.1016/j.tws.2020.107407.

Su, Z., Meng, J. and Su, Y. (2023), "Application of SiO_2 nanocomposite ferroelectric material in preparation of trampoline net for physical exercise", *Adv. Nano Res.*, **14**(4), 355-362. https://doi.org/10.12989/anr.2023.14.4.355

Xia, J., Jafari, G.S. and Ghoroughi, F. (2024), "New method environment for art design of nanocomposite brick facade of the building", *Steel Compos. Struct.*, **51**(5), 499-507. https://doi.org/10.12989/scs.2024.51.5.499

Yahea, H.T. and Majeed, W.I. (2021), "Free vibration of laminated composite plates in thermal environment using a simple four variable plate theory", *Compos. Mater. Eng.*, **3**(3), 179-199. https://doi.org/10.12989/cme.2021.3.3.179.

Yang, J., Wu, H. and Kitipornchai, S. (2017), "Buckling and postbuckling of functionally graded multilayer graphene platelet-reinforced composite beams", *Compos. Struct.*, **161**, 111-118. https://doi.org/10.1016/j.compstruct.2016.11.048

Yaylaci, M. (2022), "Simulate of edge and an internal crack problem and estimation of stress intensity factor through finite element method", *Adv. Nano Res.*, **12**(4), 405-414. https://doi.org/10.12989/ANR.2022.12.4.405

Zhang, Y., Teng, J., Huang, J., Zhou, K. and Huang, L. (2022), "Free and forced vibration analyses of functionally graded graphene-nanoplatelet-reinforced beams based on the finite element method", *Materials*, **15**(17), 6135. https://doi.org/10.3390/ma15176135

CC